PLOS ONE

RESEARCH ARTICLE

Chromodomain mutation in *S. pombe* Kat5/Mst1 affects centromere dynamics and DNA repair

Tingting Li[¤a], Ruben C. Petreaca[¤b], Susan L. Forsburg*

Program in Molecular & Computational Biology, Department of Biological Sciences, University of Southern California, Los Angeles, CA, United States of America

¤a Current address: Advanced Cell Diagnostics, A Bio-Techne Brand, Newark, CA, United States of America
¤b Current address: The Ohio State University, Marion, OH, United States of America
* forsburg@usc.edu

Check for updates

OPEN ACCESS

Citation: Li T, Petreaca RC, Forsburg SL (2024) Chromodomain mutation in *S. pombe* Kat5/Mst1 affects centromere dynamics and DNA repair. PLoS ONE 19(4): e0300732. https://doi.org/10.1371/journal.pone.0300732

Editor: Arthur J. Lustig, Tulane University Health Sciences Center, UNITED STATES

Received: June 28, 2023

Accepted: March 4, 2024

Published: April 25, 2024

Copyright: © 2024 Li et al. This is an open access article distributed under the terms of the Creative Commons Attribution License, which permits unrestricted use, distribution, and reproduction in any medium, provided the original author and source are credited.

Data Availability Statement: All strains and other reagents are available to other investigators upon request. All data are provided within figures and manuscript. Other data have been deposited to BioProject (accession number PRJNA975936) in the NCBI BioProject database (https://www.ncbi.nlm.nih.gov/bioproject/975936).

Funding: This work was supported by NIH R35 GM118109 to SLF. The funders had no role in study design, data collection and analysis, decision to publish, or preparation of the manuscript.

Abstract

KAT5 (*S. pombe* Mst1, human TIP60) is a MYST family histone acetyltransferase conserved from yeast to humans that is involved in multiple cellular activities. This family is characterized in part by containing a chromodomain, a motif associated with binding methylated histones. We show that a chromodomain mutation in the *S. pombe* Kat5, *mst1-W66R*, has defects in pericentromere silencing. *mst1-W66R* is sensitive to camptothecin (CPT) but only at an increased temperature of 36˚C, although it is proficient for growth at this temperature. We also describe a de-silencing effect at the pericentromere by CPT that is independent of RNAi and methylation machinery. We also show that *mst1-W66R* disrupts recruitment of proteins to repair foci in response to camptothecin-induced DNA damage. Our data suggest a function of Mst1 chromodomain in centromere heterochromatin formation and a separate role in genome-wide damage repair in CPT.

Introduction

Kat5 is a member of the MYST family histone acetyltransferases (HATs), and is an essential protein conserved across eukaryotes (rev. in [1, 2]). It is known as Mst1 in *S. pombe*, Esa1 in *S. cerevisiae*, and TIP60 in mammals (rev. in [3, 4]). In humans, TIP60 has also been identified as a tumor suppressor (rev. in [5, 6]) and as a therapeutic drug target (rev. in [7]). Kat5 functions as the catalytic subunit of a multi-protein complex called NuA4, and acetylates a number of different histone residues (rev. in [8]). NuA4 functions in coordination with the histone remodeling complex Swr1, which is responsible for incorporation of the histone variant H2A.Z into chromatin (rev. in [9]). Kat5 has pleiotropic functions in a wide variety of nucleic acid transactions, including transcriptional regulation, chromosome segregation and DNA double strand break (DSB) repair (rev. in [4]). In addition, some studies suggest that Kat5 may also acetylate non-histone proteins including ATM and the ssDNA binding protein RPA [10, 11].

In multiple organisms, Kat5 contributes to heterochromatin formation. For example, in mouse cells, TIP60 localizes at the pericentromeric region and is required for proper

Competing interests: The authors have declared that no competing interests exist.

chromosome segregation [12]. In *S. pombe*, Mst1 acetylation of H3K4 contributes to the switch between two H3K9^{me} bound chromodomain proteins: the RITS complex component Chp1, and the HP1 protein orthologue Swi6 [13]. In addition, Mst1 also interacts with CENP-B-like protein Cbh1, suggesting a potential role at the centromere [14].

The N-terminus of Kat5 acetyltransferase itself contains the chromodomain, a motif that potentially binds to methylated lysines in histone proteins [15]. In human cells, TIP60 binds to histone H3K9^{me} at DSBs to facilitate repair [16]. Our previous work showed that *S. pombe* Mst1 binding near DSB depends on Clr4, the H3K9 methyltransferase [17]. Interestingly, the chromodomain motif is preserved in the budding yeast Esa1 protein, although H3K9 methylation is missing in that system.

Studies in various organisms have shown that Kat5 acetyltransferase contributes to DNA damage repair and Kat5 mutations have been identified in many cancers [18]. There is evidence that the recruitment of histone variant H2A.Z and its subsequent acetylation by Kat5 are essential early in the DNA damage response [19–22]. Kat5 is responsible for the turnover of H2A.Z via acetylation [23–27]. Additionally, Kat5 is responsible for the acetylation of the damage specific phosphorylated histone variant γ-H2A(X) that promotes its turnover [28–31]. NuA4 acetylation on ssDNA binding protein RPA also regulates resection at DSB [11]. This activity may be important to activate the homologous recombination pathway as opposed to other types of repair [32, 33]. Our previous study showed that Mst1 in *S. pombe* contributes to efficient resection at DSB through H2A.Z [17]. We further showed that the Clr4 H3K9 methyltransferase contributes to recruitment of Mst1 at a DSB. NuA4 in *S. pombe* has also been linked to proper repair of damage created by Camptothecin (CPT), a topoisomerase poison that causes replication fork breakage [34].

In this study, we investigated the contribution of the chromodomain motif to Mst1 activity in fission yeast. To facilitate comparisons across systems, we constructed an allele *mst1-W66R* in a highly conserved residue that corresponds to a mutation previously analyzed in *S. cerevisiae* [35]. We show that *mst1-W66R* is viable at all temperatures but is defective in heterochromatin silencing at the pericentromere domain. This mutant shows temperature-dependent defects in resistance to CPT treatment and unexpectedly, we find that CPT also destabilizes silencing. Our data further suggest that Mst1 is required for the global response to CPT and assembly of appropriate repair proteins.

Results

Construction and characterization of a chromodomain mutation in Mst1

All Kat5 family proteins have a chromodomain in the N-terminus, which is presumed to bind methylated histones (rev. in [15]). There is evidence from human cells that the chromodomain targets Kat5 to methylated H3K9 [16, 36, 37]. This histone modification is associated with heterochromatin assembly [13, 14] and has been linked to DSB repair (rev. in [38]). Our previous work demonstrated that fission yeast Mst1 contributes to resection and recruitment of repair proteins to DSBs, and also showed that this depends upon the H3K9 methyltransferase Clr4 [17], consistent with a canonical role for the Mst1 chromodomain.

Interestingly, the budding yeast *S. cerevisiae* lacks H3K9 methylation, although its Kat5 orthologue Esa1 preserves the conserved chromodomain. A mutation in the highly conserved residue in the chromodomain of *S. cerevisiae* Esa1 W66R causes impaired histone H4 acetylation and sensitivity to the genotoxin camptothecin [35].

We constructed the equivalent mutation in *S. pombe* to facilitate comparison between a system that maintains H3K9 methylation, and one that lacks it: the allele *mst1*-W66R that

corresponds to *S. cerevisiae esa1-W66R* [35] (Fig 1A). This residue is also conserved in all *S. pombe* chromodomain proteins (S1 Fig).

We compared the phenotypes of *mst1-W66R* to those of the *mst1-L344S*, a previously characterized temperature sensitive allele which has a number of defects even under permissive conditions [14, 17]. Unlike the *mst1-L344S* allele which harbors a mutation in the catalytic domain of the enzyme (Fig 1A), the *mst1-W66R* mutant is viable at all temperatures, with no evidence for temperature sensitivity (Fig 1B). Previously we showed that *mst1-L344S* at the permissive temperature is extremely sensitive to genotoxic stressors including the radiomimetic bleomycin, the alkylating agent methyl methanesulfonate (MMS), nucleotide starvation drug hydroxyurea (HU), and topoisomerase (Top1) inhibitor camptothecin (CPT) [14]. We investigated whether *mst1-W66R* shows any similar sensitivities. We observed that *mst1-W66R* was not sensitive to bleomycin, HU, or MMS at any temperature. Curiously, we observed sensitivity to CPT, but only at 36˚C (Fig 1B). CPT captures Top1 complexes on the DNA (rev. in [39]) which is associated with increased double strand breaks not only during DNA replication [40], but in transcription as well [41]. The fact that both *mst1* alleles show sensitivity to CPT underscores the role of Mst1 in DNA double strand break repair.

Our previous work showed that loss of the H3K9 methyltransferase Clr4 leads to reduced localization of Mst1 and the HR protein Rad51 to DSBs, and delayed resection [17]. Therefore, we investigated whether the *W66R* chromodomain mutation impairs resection and recruitment of a DSB. Because *mst1-W66R* CPT sensitivity is temperature sensitive, we examined these dynamics at 36˚C. As before, we used a strain containing an HO-inducible DSB adjacent to a lacO array that recruits mCherry-lacI, and CFP-tagged Rad52 [42]. The strain produces persistent DSBs [43]. Following break induction, the two ends are first resected, then repair factors including Rad52 are recruited to the break. Loss of the mCherry signal corresponds to resection while an increased CFP signal indicates that RAD52-CFP has been recruited to the break. We imaged both wild-type and *mst1-W66R* cells after break induction at 36˚C (Fig 1C; see materials and methods). We compared this to our prior study using *mst1-L344S* at permissive temperature, in which we observed resection defects [17]. We find that, similarly to *mst1-L344S*, the cherry signal was maintained in *mst1-W66R*, suggesting a reduced efficiency of resection. However, localization of the Rad52 protein to the DSB increases over time in *mst1-W66R*, whereas it declines in *mst1-L344S*, suggesting a defect in Rad52-CFP recruitment for *mst1-L344S* but not *mst1-W66R*. Thus, *mst1-W66R* also has a DSB repair defect but does not simply phenocopy *mst1-L344S*.

mst1-W66R does not affect DNA damage transcription response

Because Mst1 has a role in transcriptional regulation [44], we investigated whether the temperature-dependent phenotypes in *mst1*-W66R are linked to changes in transcription specifically of DNA damage repair genes. We performed mRNA-sequencing to compare the transcription profile of *mst1-W66R* cells at 36˚C compared to wild type. Using a threshold of $|\log FC| > 1.5$ and p-value<0.05, we found only 25 genes were significantly up-regulated and 27 significantly were down-regulated in *mst1-W66R* compared to wild type and most of these differentially expressed genes were non-coding RNAs (S2A Fig and S2 Table).

Next, we examined the transcriptional response in CPT-treated *mst1-W66R*. We observed that 48 genes were significantly up-regulated and 128 were significantly down-regulated in CPT-treated *mst1-W66R* compared to untreated (S2B Fig and S2 Table). Of these, 29 up-regulated genes in *mst1-W66R* were also up-regulated in wild type with CPT, and 35 down-regulated genes in *mst1-W66R* were also down-regulated in wild type with CPT (S2 Table). Most of the genes that were differentially expressed in CPT-treated *mst1-W66R* compared to wild type

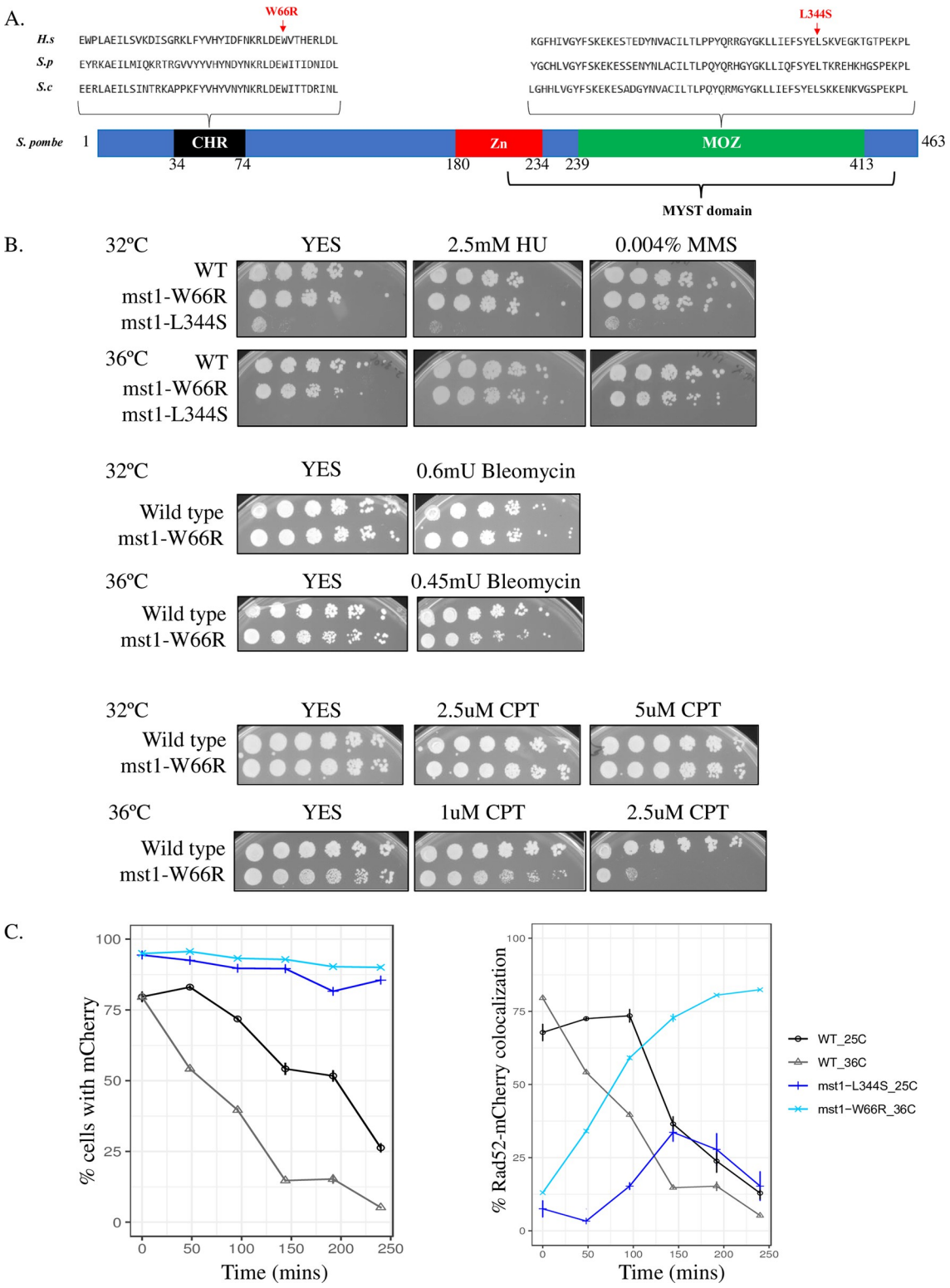


Fig 1. *mst1-W66R* allele characterization. (A) The alignment of *H. sapiens* TIP60, *S. cerevisiae* Esa1 and *S. pombe* Mst1. The mutation at W66 (*S. pombe* and *S. cerevisiae* coordinates) and L344 (*S. pombe* coordinates) are marked with the arrow. (B) The *mst1-W66R* shows sensitivity to CPT at 36˚C. Cells were grown in YES media overnight at 32˚C then 5X serial dilutions were spotted onto YES plates or YES plates containing HU, MMS, Bleomycin or CPT. Plates were incubated at 32˚C or 36˚C and photographed after 4 days. (C) **Left**: Percentage of cells with HO-induced mCherry foci over 240 minutes in wild type and *mst1-W66R* cells at 36˚C. **Right**: Percentage of cells with colocalized Rad52-CFP and HO-induced mCherry foci over 240 minutes in *mst1-W66R* cells.

https://doi.org/10.1371/journal.pone.0300732.g001

are involved in metabolism. Overall, we found that metabolic gene sets were enriched in CPT-treated *mst1-W66R* compared to untreated from KEGG analysis (S2C Fig), while aminoacyl-tRNA biosynthesis was also found depleted in CPT-treated *mst1-W66R* (S2D Fig). GO analyses and GSEA analyses were also conducted but no gene sets passed the threshold. These data indicate that the disruption in the CPT response is not predominantly due to disruption of transcription of damage response genes, nor a generalized transcription defect.

Temperature specific silencing defects in *mst1-W66R*

Previous studies have suggested that in some systems, the conserved KAT5 chromodomain binds to H3K9^{me} histone [16, 35, 36]. In fission yeast, Clr4 methylates H3K9 that is essential for assembly of pericentric heterochromatin, which in turn contributes to faithful chromosome segregation (rev. in [45]). To investigate whether the Mst1 chromodomain contributes to heterochromatin function, we examined chromosome segregation in *mst1-W66R* at 32˚C and at 36˚C. We observed that cells showed modestly reduced colony size, increased rates of chromosome mis-segregation and lagging chromosomes, and increased thiabendazole (TBZ) sensitivity, most noticeably at 36˚C (Fig 2A). This suggests an impairment in centromere function particularly at higher temperature.

We next examined whether *mst1-W66R* affects heterochromatin silencing at the centromere region, which depends on H3K9 methylation (rev. in [46]). Prior evidence shows that heterochromatin silencing is intrinsically temperature sensitive even in wild type cells [47, 48]. We utilized strains that contain a *ura4*$^{+}$ reporter gene integrated at the outer repeat *otr1L(dh)* of centromere 1 (Fig 2B) [49]. Cells that fail to silence *ura4*$^{+}$ properly can grow in non-selective media, but are inviable in media containing 5-fluoro-orotic acid (5-FOA). Wild type cells containing the reporter gene showed growth in both non-selective media and media containing 5-FOA, indicating that silencing at the centromere is intact. In contrast, the control strain *swi6-L315K* was killed by 5-FOA [50]. *mst1-W66R* showed similar silencing defects as *swi6-L315K* at both temperatures, suggesting that the Mst1 chromodomain contributes to the silencing of the outer pericentromeric regions.

Temperature dependent CPT sensitivity among heterochromatin mutants

Since *mst1-W66R* showed a temperature-specific sensitivity in CPT as well as centromere silencing and increased chromosome mis-segregation at 36˚C, we wondered whether these phenotypes were linked in some way. We investigated whether known heterochromatin mutants also show increased CPT sensitivity at higher temperature. We examined *clr4Δ*, disrupting the H3K9 methyltransferase that promotes heterochromatin formation [51, 52]; *swi6Δ*, disrupting the heterochromatin protein HP1 that binds to H3K9 methylated histone [51]; and *dcr1Δ*, which removes Dicer protein that promotes RNAi required for methylation [53]. We observed that the individual heterochromatin mutants all showed modest CPT sensitivity at higher temperature, but not as dramatic as *mst1-W66R* (Fig 3).

We constructed double mutants between these heterochromatin protein mutants and *mst1-W66R*. We found that *clr4Δ*, *swi6Δ* and *dcr1Δ* double mutants showed mild synthetic defects with *mst1-W66R* at 32˚C which were increased at 36˚C compared to *mst1-W66R* alone (Fig 3 and S3A Fig). This suggests that the *mst1-W66R* CPT phenotype is at least partly independent of H3K9^{me} by Clr4, and independent of its effects on heterochromatin.

Next, we asked whether CPT treatment itself affects heterochromatin silencing. We performed reverse-transcriptase PCR on the *ura4*$^{+}$ gene inserted at outer repeats of chromosome I (Fig 4, S1 Raw images). At 32˚C, the signal at the outer repeat was only 0.2 times of that at the euchromatic locus, consistent with silencing. Intriguingly, after four-hour CPT treatment, the

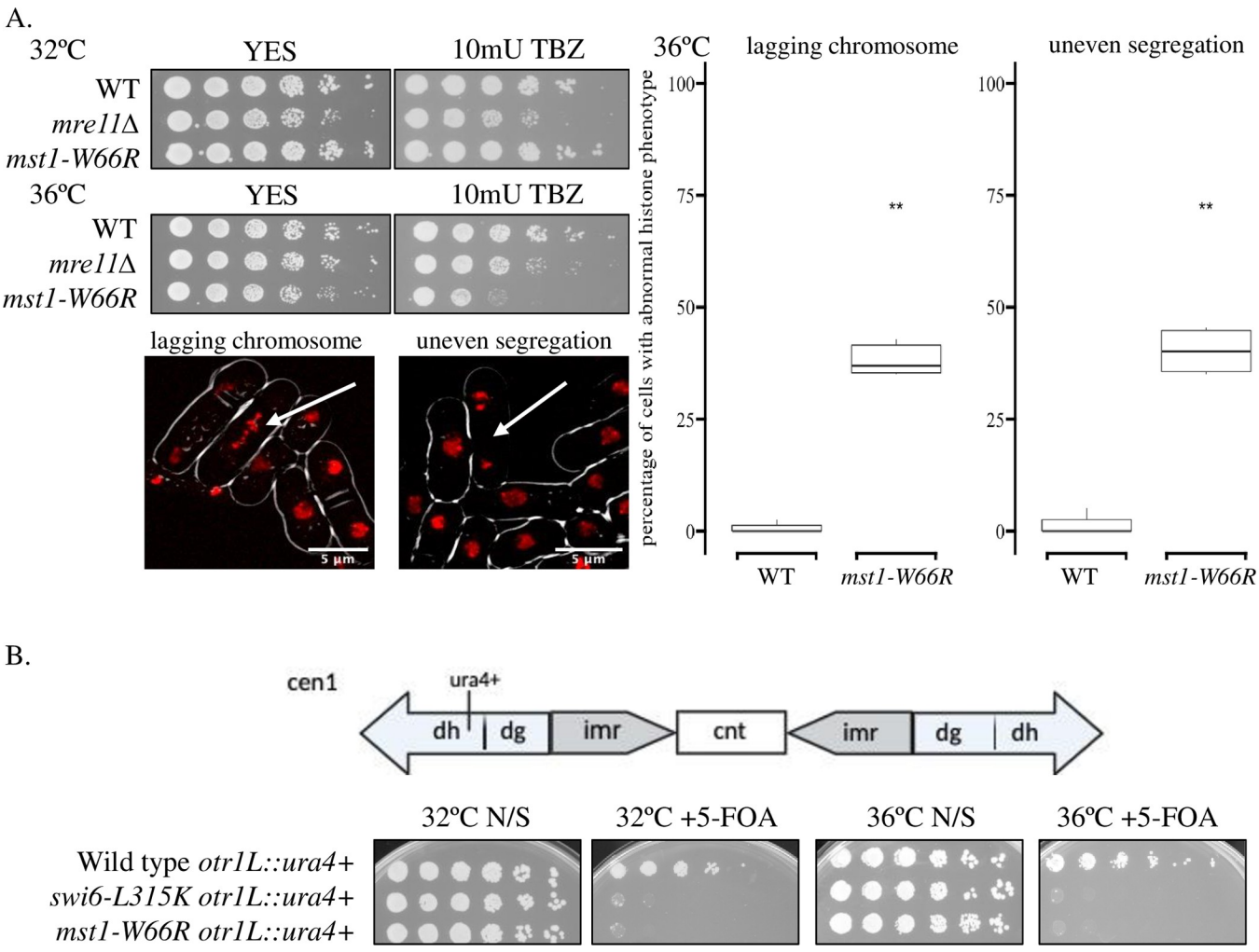


Fig 2. *mst1-W66R* showed temperature specific silencing defects. (A) **Left Top:** *mst1-W66R* growth in TBZ at 32˚C and 36˚C. *mre11Δ* as negative control. **Left Bottom:** Representatives of *mst1-W66R* cells with Hht1-mRFP showing lagging chromosome (left) and uneven segregation phenotype (right). **Right:** percentage of wild type and *mst1-W66R* cells with lagging chromosome or uneven segregation phenotypes at 36˚C. (B) **Top:** Schematic of the *ura4*$^+$ marker in the *cen1 dh* repeats. **Bottom:** expression of centromere Ura4 in different mutants at 32˚C or 36˚C was determined by sensitivity to 5-FOA. N/S, non-selective (Uracil+) medium.

https://doi.org/10.1371/journal.pone.0300732.g002

expression of *ura4*$^+$ at the outer repeats increased to 0.8 times of that at the euchromatic locus, suggesting that CPT can partially disrupt silencing.

Previous studies showed that *S. pombe* cells lose pericentromere silencing at higher temperature, correlating with loss of RNAi activity as Dicer protein is exported out of nuclei [47, 48, 54]. Consistent with this, we observed that untreated wild type cells at 36˚ showed higher expression of outer repeats compared to 32˚C. CPT treatment further increased this expression. Thus, increased temperature and CPT appear to have cumulative effects on silencing. Untreated *swi6Δ* and *mst1-W66R* strains show similar expression. Following 4hr CPT treatment, outer repeat expression in *swi6Δ* was slightly higher than that in wild type cells with CPT treatment. We observed that *mst1-W66R* cells at 36˚C had increased expression from outer repeats compared to wild type cells at 36˚C, but this was not further induced by CPT treatment.

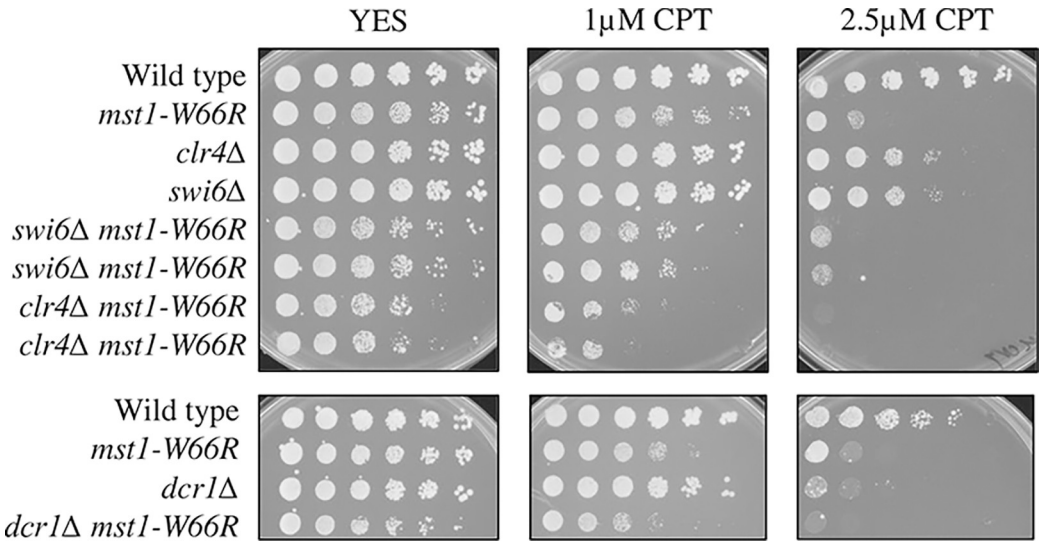


Fig 3. Heterochromatin mutants show sensitivity to CPT at 36˚C. *clr4Δ*, *swi6Δ*, *dcr1Δ* and the double mutants with *mst1-W66R* showed sensitivity to CPT at 36˚C. Cells were grown in YES media overnight at 32˚C then 5X serial dilutions were spotted onto YES plates or YES plates containing CPT. Plates were incubated at 36˚C and photographed after 4 days.

https://doi.org/10.1371/journal.pone.0300732.g003

Mst1-W66R is dominant negative

We wondered whether *mst1-W66R* has a dominant negative effect. To address this hypothesis, we transformed *mst1-W66R* cells with an episomal plasmid expressing wild type Mst1 under the native promoter and Leu+ selective marker (S3B Fig). Even with the wild type Mst1 expressed in *mst1-W66R*, cells still showed sensitivity to CPT at 36˚C, although not quite to the same extent. Increasing expression of *mst1+* on a plasmid with the *nmt1* promoter showed additional rescue (data not shown), consistent with a dominant negative phenotype.

mst1-W66R is required to recruit repair proteins in CPT

We speculated that the CPT sensitivity in *mst1-W66R* might be due to an additional function in repair of CPT-induced damage independent of the pericentromere silencing defect. We

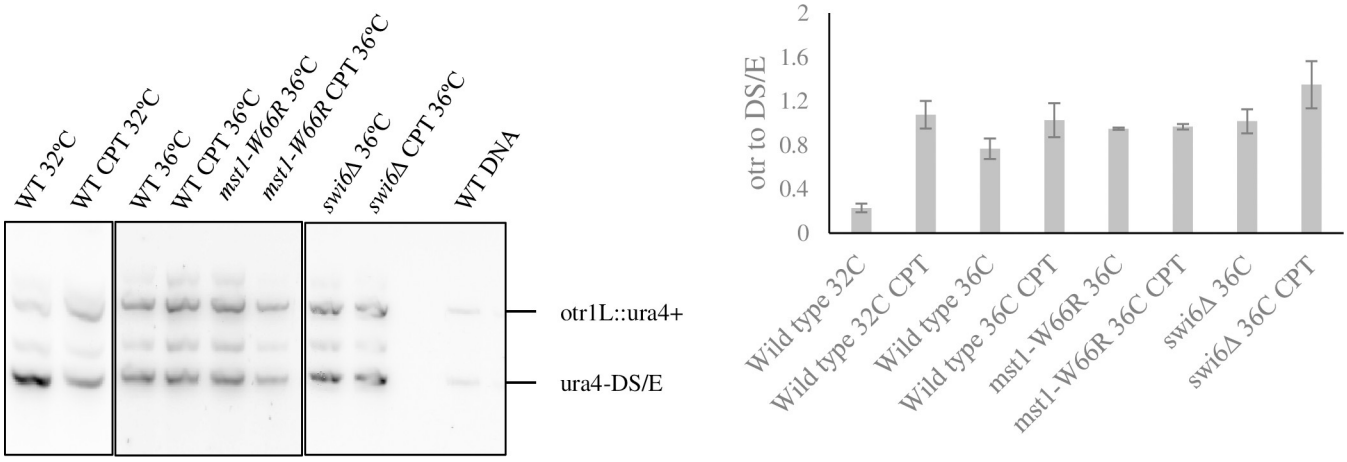


Fig 4. CPT de-silenced centromere but independent of Mst1. *ura4+* expression in *cen1L(dh)* measured using RT-PCR with or without four-hour 15μM CPT treatment at 32˚C or 36˚C. Signals were normalized to expression of the *ura4-DS/E* minigene at the normal (euchromatic) locus.

https://doi.org/10.1371/journal.pone.0300732.g004

examined the response of *mst1-W66R* cells to CPT treatment by monitoring recruitment of repair proteins to characteristic repair foci, following four-hour treatment with CPT at 36˚C. We first examined at the localization of RPA which binds single strand DNA (ssDNA) (Fig 5A). Untreated wild type and *mst1-W66R* cells have a similar low percentage of cells with RPA foci. However, after treatment with 5μg/mL CPT at 36˚C, significantly more wild type cells (58.57%) have foci than *mst1-W66R* cells (26.76%) (S3 Table). The RPA foci in *mst1-W66R* were distributed throughout the nucleus, suggesting that RPA is not preferentially localized at the centromere, which is typically peripheral (S4A Fig).

We next investigated the recruitment of proteins involved in fork rescue and homologous recombination. Rad52 is associated with various recombination pathways including single-strand annealing (SSA), homologous recombination (HR), and synthesis dependent strand annealing (SDSA) (rev. in [55]) and is thought to facilitate RPA displacement [56] (Fig 5B). We observed that 10% of cells have Rad52 foci in both wild type and *mst1-W66R* background in untreated cells. Upon CPT treatment, there was a modest increase to about 25% of wild type cells showing Rad52 foci. However, in *mst1-W66R* treated with CPT, there was no increase of Rad52 signal, and the percentage of cells with Rad52 foci remained at about 10% (S3 Table).

We next investigated the role of Rad54, which functions downstream of Rad51 in homologous recombination and fork reversal [57, 58] (Fig 5C). In untreated cells, both wild type and *mst1-W66R* showed similar levels of Rad54-GFP foci, in around 10–15% of the cells. However, in contrast to our observations with RPA and Rad52, both wild type and *mst1-W66R* cells induced Rad54 foci to about 50% after CPT treatment.

Together, these imaging data show a distinct pattern of repair protein recruitment in *mst1-W66R*. To further understand these phenotypes and how they may reflect CPT sensitivity, we took a candidate approach to determine the involvement of known repair pathways in CPT response.

Interactions with known repair pathways

We investigated the genetic interaction between *mst1-W66R* and selected mutants that are known to facilitate CPT response, by constructing double mutants and performing growth assays on plates (Fig 6). We tested interactions with *tdp1Δ*, encoding the phosphodiesterase that removes Top1 adducts [59]; *mre11Δ*, encoding the nuclease required for resection at breaks [60]; and *mus81Δ*, an endonuclease required for fork reversal following CPT treatment [61]. Additionally, recent studies have implicated XPF nucleases in cleavage during CPT response in non-replicating cells [62] so we examined *rad16*Δ (part of the XPF nuclease; [63]). We also examined *rad2Δ*, which encodes the FEN-1 endonuclease [64]. Recent research in human cells showed FEN1 endonuclease is epistatic with XPF for CPT damage repair [41].

We observed a modest reduction in colony size on YES at 36˚C for *mst1-W66R mus81Δ* or *mst1-W66R mre11Δ*, compared to the single mutants, indicating a synthetic phenotype even in the absence of exogenous genotoxic stress. The *mus81Δ* single mutant is extremely CPT sensitive even at 0.1μM CPT, and the double mutant was completely inviable on CPT. We observed that *mst1-W66R mre11Δ* and *mst1-W66R tdp1Δ* were more sensitive than either single mutant to low doses of CPT. These data suggest the role of *mst1-W66R* is separate from *mre11Δ*, *mus81Δ* or *tdp1Δ* since the combined effect is more dramatic than either parent.

The *rad16Δ* mutant shows minimal CPT sensitivity, while the double mutant *rad16Δ mst1-W66R* resembles *mst1-W66R*. While *rad2Δ* has modest CPT sensitivity by itself, again the double mutant resembles *mst1-W66R* alone. However, *rad16Δ rad2Δ* double mutant has increased CPT sensitivity relative to either single mutant, suggesting that they work in separate pathways.

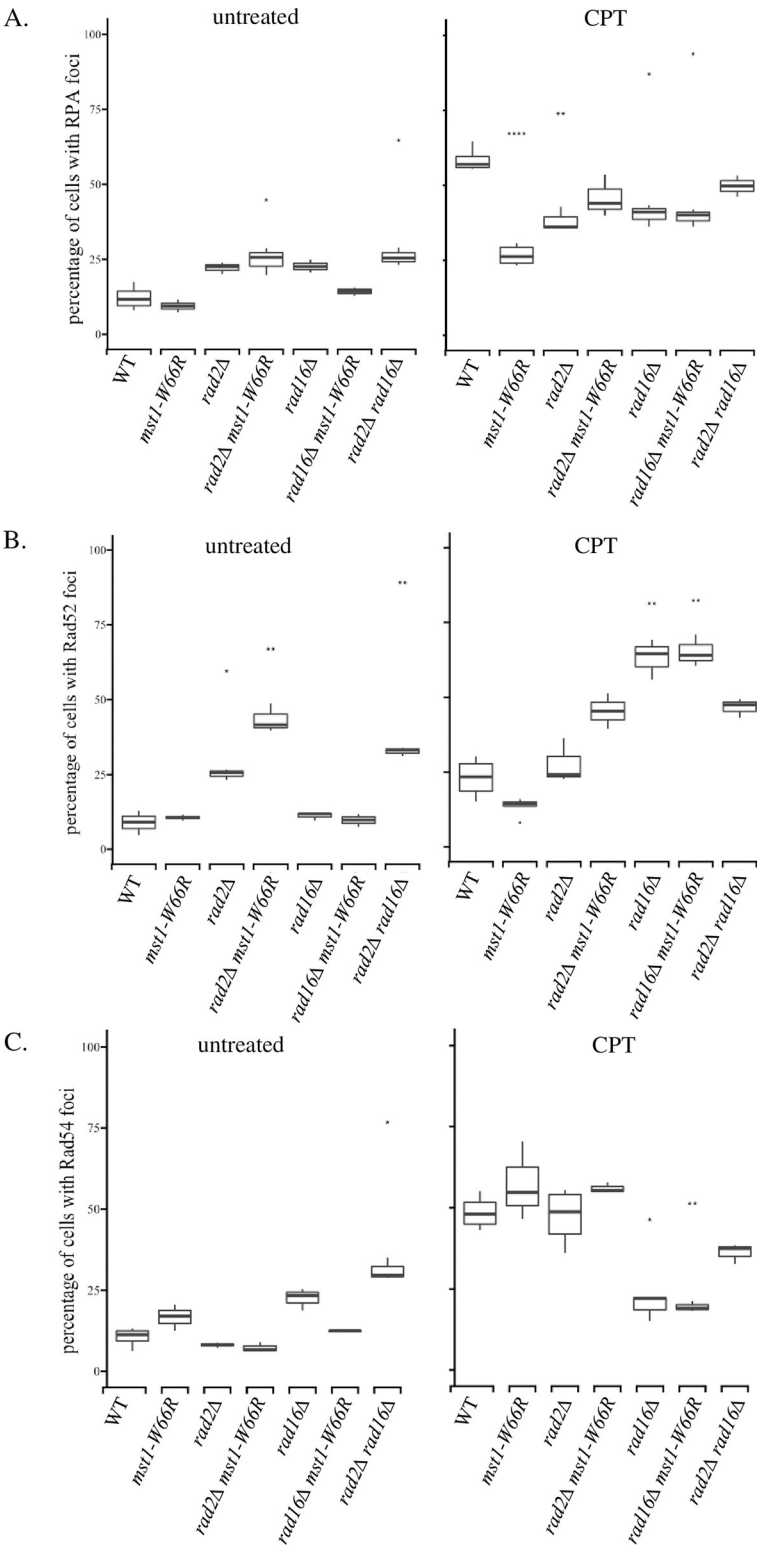


Fig 5. The *mst1-W66R* mutants affect recruitment of repair proteins at 36˚C in CPT Percentage of cells with (A) RPA (Rad11) (B) Rad52 and (C) Rad54 foci in WT, *mst1-W66R*, *rad2Δ*, *rad2Δ mst1-W66R*, *rad16Δ*, *rad16Δ mst1-W66R* and *rad2Δ rad16Δ*. The bold line in each box represents median. Asterisks represent percentage of cells with foci is significantly different than that in WT (*: p<0.05, **: p<0.01, ****: p<5e-05 Mann-Whitney Test).

https://doi.org/10.1371/journal.pone.0300732.g005

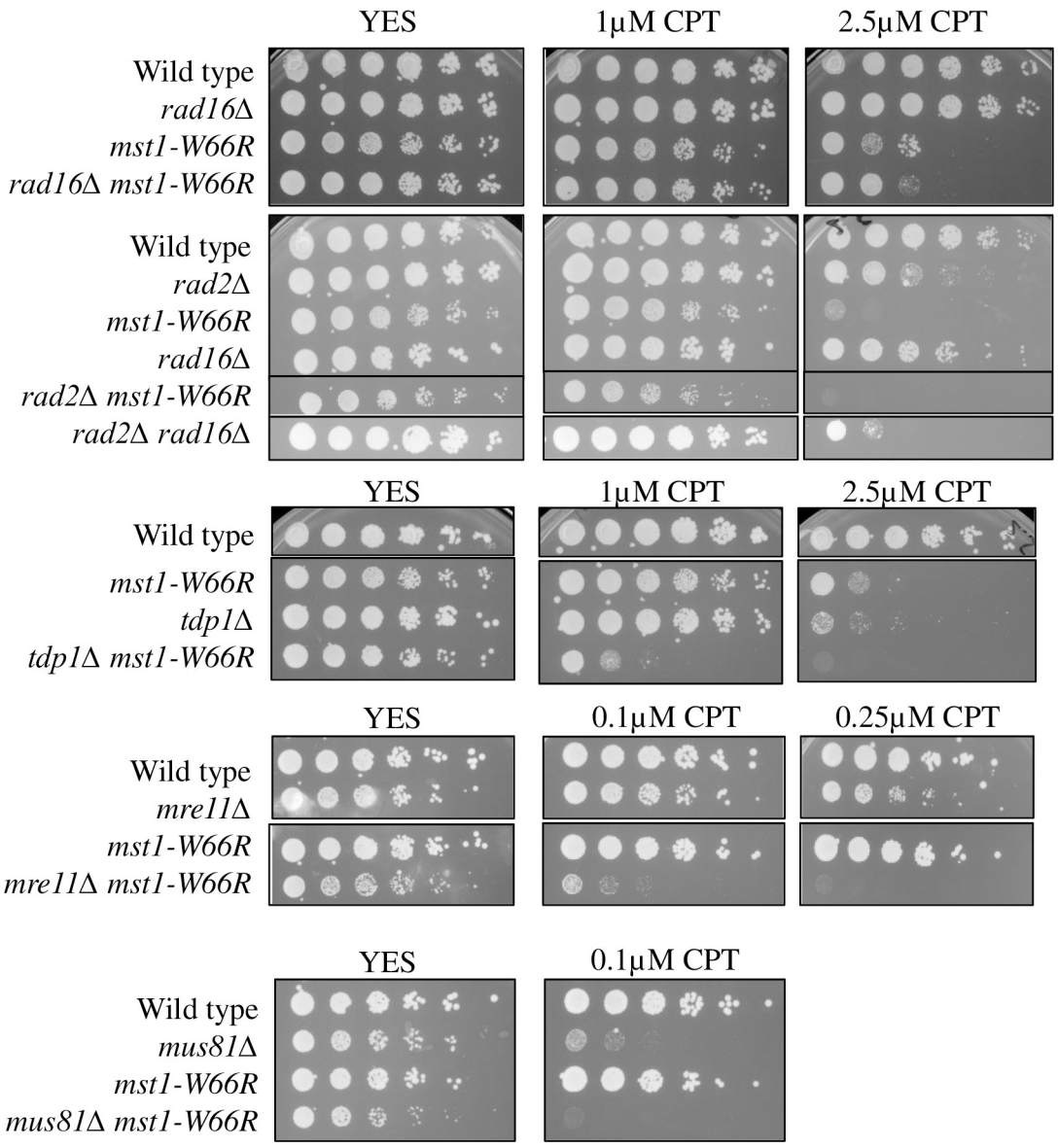


Fig 6. Genetic interaction between *mst1-W66R* and mutants involved in Top1cc removal. *rad16Δ*, *rad2Δ*, *tdp1Δ*, *mre11Δ*, *mus81Δ* and the double mutants with *mst1-W66R* sensitivity to CPT at 36˚C. Cells were grown in YES media overnight at 32˚C then 5X serial dilutions were spotted onto YES plates or YES plates containing CPT. Plates were incubated at 36˚C and photographed after 4 days.

https://doi.org/10.1371/journal.pone.0300732.g006

Epistatic interactions of Mst1 with XPF1 and FEN1 endonclease

Since the *mst1-W66R* CPT growth phenotype is epistatic to both *rad16Δ* and *rad2Δ*, we investigated how these mutants interact by examining recruitment of RPA, Rad52 and Rad54 to repair foci.

Untreated *rad16Δ* cells have more RPA foci than wild type, but this increase was partly rescued in the *mst1-W66R rad16Δ* double mutant (Fig 5A). However, following a four-hour CPT treatment, the percentage of cells with RPA foci increased to about 40% in both single and double *rad16Δ* mutants (S2 Table). Although this percentage was not as high as in wild type, it is significantly higher than the RPA foci observed in CPT-treated *mst1-W66R* cells.

Untreated *rad16Δ*, *mst1-W66R*, and wild type all showed similar percentages of Rad52 foci (Fig 5B). However, following CPT treatment, *rad16Δ* showed dramatic increase of cells with Rad52 compared to wild type. A similar high percentage was also observed in the *rad16Δ mst1-W66R* double mutant. Notably, contrasting with the Rad52 results, there was no increase in Rad54 foci upon CPT treatment in either *rad16Δ* and *rad16Δ mst1-W66R* (Fig 5C). Despite the absence of CPT sensitivity in *rad16Δ*, this mutation dramatically changes the recruitment of Rad52 and Rad54, in opposite directions.

We examined protein recruitment in *rad2Δ* single and double mutants. Similarly to *rad16Δ*, *rad2Δ* mutants had modestly increased cells with RPA foci than wild type without treatment (Fig 5A). *rad2Δ* also partially rescued the defects of recruiting RPA foci in *mst1-W66R* upon CPT treatment. However, like *mst1-W66R*, *rad2Δ* mutants showed very little increase in Rad52 protein recruitment following CPT treatment when comparing to untreated (Fig 5B and S2 Table). However, recruitment of Rad54 foci is unchanged in *rad2Δ* mutants compared to wild type (Fig 5C). Thus, *rad2Δ* has opposite effects on repair focus formation compared to *rad16Δ*.

Finally, we examined *rad2Δ rad16Δ*, which is strikingly more sensitive to CPT than either single mutant. The double mutant showed slightly more cells with RPA foci when treated with CPT (Fig 5A). Rad52 foci were notably lower in *rad2Δ rad16Δ* than the *rad16Δ* or *rad16Δ mst1-W66R* strains. (Fig 5B and 5C). Similarly, the accumulation of Rad54 foci in *rad2Δ rad16Δ* was intermediate between the levels observed for the two single mutants in CPT. The data suggest that Rad2 and Rad16 in *S. pombe* are not in a common pathway for CPT repair response.

Discussion

The Kat5 acetyltransferase in *S. pombe* Mst1 is the catalytic subunit of the NuA4 histone acetyltransferase complex, and makes pleiotropic contributions to genome stability (rev. in [4, 63]). In our previous reports, we showed that Mst1 is essential for viability and facilitates acute DSB repair by promoting long-range resection that depends on Exo1 [14, 17]. We found that Mst1 binding to DSB requires Clr4, the H3K9 methyltransferase in *S. pombe* [17, 51, 52]. This is consistent with data from metazoans that indicate a role for H3K9^{me} in targeting Kat5 proteins to sites of DNA damage [16, 36, 37].

Curiously, the *S. cerevisiae* Kat5 orthologue Esa1 also contains a conserved chromodomain, despite the absence of H3K9^{me} and its associated heterochromatin in this organism [65]. The chromodomain mutation *esa1-W66R* creates sensitivity to various genotoxins, suggesting a role in repair response that is independent of H3K9^{me} [35]. We constructed the equivalent fission yeast *mst1-W66R* to examine H3K9-dependent and independent roles for this domain in fission yeast.

S. pombe mst1-W66R is not sensitive to MMS, HU, or DSB-inducing drug Bleomycin, and unexpectedly only showed sensitivity to CPT at 36˚C (Fig 2). CPT leads to damage by stalling the topoisomerase I cleavage complex (Top1cc) on DNA (rev. in [39]), leading to S-phase dependent DNA breaks [66]. CPT also affects formation of DNA-RNA hybrids due to replication-transcription collision [41]. Our data show that *mst1-W66R* has defects in long-range resection but can still (albeit slowly) recruit recombination protein Rad52 to an induced DSB, suggesting a long-range resection independent but Rad52-dependent pathway is activated. We posit this might be due to single strand annealing or MMEJ, but this will require further examination.

In contrast to the hypomorph *mst1-L344S*, we observed only minimal changes in transcription in *mst1-W66R*, none of which obviously linked to the CPT repair response. Of 52

differentially expressed genes, only one of them overlaps with the differentially expressed genes in *mst1-L344S* [44]. This suggests that the *W66R* allele does not substantially affect general transcriptional regulation by Mst1. We also compared the transcriptome in CPT-treated *mst1-W66R* to that of the untreated one, and most of the differentially expressed genes were related to metabolism. We conclude that damage-induced transcription is not the major regulator of the CPT response in *mst1-W66R*.

Methylation of H3K9 by Clr4 and subsequent binding of chromodomain proteins Swi6/HP1 and Chp1 define the pericentromeric heterochromatin in *S. pombe* (rev. in [45]). Mst1 has previously been shown to contribute to recruitment of Swi6 by acetylating H3K4 [13]. We found that *mst1-W66R* has defects in silencing at outer repeats of centromere starting at 32˚C and increased at 36˚C. (Figs 2B and 4). Loss of silencing typically correlates to centromere dysfunction leading to disruptions in chromosome segregation and sensitivity to the microtubule poison TBZ [47, 67, 68], rev. in [46]) and we observed both of these phenotypes (Fig 2).

Assembly of the pericentromere heterochromatin via RNAi machinery is temperature sensitive [45, 48]. This likely reflects the mislocalization of the Dicer protein Dcr1 at higher temperature [54]. Although CPT is widely viewed as an S-phase specific inhibitor that blocks replication fork progression, it also affects resolution of transcription [69]. Interestingly, in addition to its role promoting heterochromatin assembly and H3K9 methylation, Dcr1 is also important to resolve DNA/RNA hybrids to reduce transcription/replication collisions [70]. We reasoned that increased transcription at the pericentromere due to temperature-dependent loss of silencing could create conditions that increase CPT sensitivity. Therefore, we hypothesized that centromere silencing defects and CPT-sensitivity phenotypes in *mst1-W66R* could be linked, and mutants affecting heterochromatin formation might also have growth defects in CPT. If this were the case, then mutations that eliminate heterochromatin formation at the pericentromere would increase CPT sensitivity. This was not what we observed: *clr4Δ*, the mutant of H3K9 methyltransferase [51, 52]; *swi6Δ*, the mutant of HP1 [51]; as well as *dcr1Δ*, the mutant of Dicer protein [53] did not affect CPT sensitivity at lower temperatures. However, all these mutants showed CPT sensitivity at 36˚C. Therefore, this CPT sensitivity is not due to increased transcription in the centromere (which occurs at all temperatures in heterochromatin mutants). This suggests that proteins important for heterochromatin establishment at centromere are also required for the proper response in CPT-induced damage repair. Importantly, we observed that heterochromatin mutants appeared less sensitive to CPT than *mst1-W66R*, while double mutants with *mst1-W66R* showed increased sensitivity to CPT relative to either single mutant. We conclude that Mst1's response to CPT-induced damage response is at least partially independent from heterochromatin formation and H3K9^{me} binding.

One possibility is that the *mst1-W66R* mutant is temperature sensitive for some of its activities, although it is clearly competent to fulfill its essential functions. However, we observe that sensitivity of *mst1-W66R* to CPT is observed even in the presence of wild type Mst1, indicating a dominant negative effect. This may be due to a conflict between wild type and mutant forms of the NuA4 complex, where the mutant complex is recruited to some sites and inhibits appropriate interactions and argues against a simple temperature sensitive defect.

We examined whether CPT treatment impacts silencing directly. Consistent with previous studies that RNAi machinery is partially impaired at restrictive temperature [47, 48], we observed reduced silencing of a reporter at 36˚C compared to 32˚C. CPT treatment modestly reduced expression at outer repeats at 32˚C. We reasoned that such de-silencing could result from -transcription collisions at the centromere, and thus inhibition of siRNA production to silence the centromere. However, expression was not further increased at 36˚C or in the *W66R* background, suggesting CPT-induced de-silencing is independent of RNAi machinery and

Mst1. Finally, CPT treatment in *swi6Δ* led to higher expression at outer repeats compared to the untreated, suggesting the CPT-induced de-silencing is also independent of heterochromatin assembly. These data suggest that CPT interferes with silencing in some other way.

The increased sensitivity of *mst1-W66R* in CPT-induced de-silencing suggests it has a role in repair of CPT-induced damage, apart from its silencing function at centromere. Indeed, we found that *mst1-W66R* disrupts recruitment of repair proteins RPA, the ssDNA binding protein; recombination protein Rad52 (Fig 5), suggesting the chromodomain of Mst1 might regulate resection at CPT-induced damage, and facilitate Rad52-mediated repair pathways. In contrast, Mst1 does not affect the recruitment of homologous recombination protein Rad54 following CPT treatment. The presence of multiple dispersed repair foci in one nucleus in *mst1-W66R* upon CPT treatment suggests that the genome-wide damage generated by CPT treatment is not limited to the centromere domain (S4B Fig). The formation of ssDNA can be driven by a variety of pathways including resection, recombination, and/or helicase uncoupling [71]. The reduction in ssDNA signal in *mst1-W66R* therefore could reflect any of these pathways but would be consistent with the reduced resection we observe in the DSB repair assay.

We constructed candidate double mutants to assess what pathways may be affected by *mst1-W66R* and assessed CPT sensitivity in chronic exposure. We find that *mst1-W66R* is epistatic to *rad16Δ* the homolog of XPF endonuclease that cleaves the 3'end of DNA-protein adducts [41, 62]. Repair of CPT damage is complex because the drug blocks Top1 in the cleavable complex and produces DSBs which are repaired during S-phase. The growth data in Fig 6A shows that the growth of the *rad16Δ mst1-W66R* double mutant is worse than *rad16Δ* single and comparative to *mst1-W66R*, though not identical, suggesting that $rad16^{+}$ has functions independent of $mst1^{+}$. However, Fig 5C shows that the *mst1-W66R* epistatic phenotype to *rad16Δ* does not extend to recruitment of repair factors to the DSB (e.g. *rad16Δ* shows the same phenotype as *mst1-W66R rad16Δ)*. Thus, the growth defects observed in Fig 6 represent Mst1-Rad16 interactions not related to recruitment of repair factors. However, the interactions between *mst1-W66R* and *rad2Δ*, the FEN-1 endonuclease known for its function in Okazaki fragment processing, do extend to recruitment of repair factors as the double mutant does have different recruitment defects than the single mutants (Fig 5), In other systems, Fen1 was shown to work in an epistasis group with XPF in CPT damage response [41, 64]. Therefore, not unexpectedly, in fission yeast *rad16Δ rad2Δ* showed increased CPT sensitivity.

We observed that both *rad16Δ* and *rad2Δ* mutants showed accumulation of RPA foci when untreated, suggesting the presence of endogenous damage. RPA foci were further induced following CPT treatment. Although *mst1-W66R* alone does not induce RPA signal, the double mutant with *rad16* shows significant increase (like the *rad16* single mutant), while the double mutant with *rad2* shows no induction. However, these mutants also diverged in their recruitment of Rad52. The *rad2Δ* cells had increased Rad52 foci in both as single and double (*mst1-W66R)* mutants when untreated, but it did not increase upon CPT treatment. In contrast, *rad16Δ* did not show accumulation of Rad52 foci when left untreated, but significantly increased the percentage after CPT treatment. We hypothesize that Mst1 repairs the genome-wide CPT-induced damage through promoting FEN1 and inhibiting XPF endonucleases. This suggests that unlike human cells, XPF endonuclease inhibits the Rad52-mediated SSA repair at CPT-induced damage in *S. pombe*, but promotes Rad54-mediated fork reversal [72]. FEN1 also does not work in the same pathway with XPF to remove R-loops induced by CPT as in human cells [41], but it facilitates the Rad52-mediated SSA while it has little impact on fork reversal.

It is interesting that the *esa1-W66R* mutant in budding yeast leads to a similar CPT phenotype despite the absence of $H3K9^{me}$ in that organism [35]. Similarly, we find that fission yeast

mst1-W66R does not phenocopy *clr4Δ* especially upon CPT treatment. One possibility is that other methylations might recruit the Mst1 chromodomain in response to CPT. There is evidence that mammalian Kat5 chromodomain has affinity to H3K4me, H3K27me, H3K36me, and H4K20me, in addition to H3K9^{me} [73]. In human cells, H3K36^{me} by SETD2 results in survival defects in CPT [74]. In *S. pombe*, cells without H4K20^{me} also show higher sensitivity to CPT. Some studies suggest that the *S. cerevisiae* Esa1 chromodomain may target unmodified histones, or RNA [75, 76]. Additionally, some evidence in *S. pombe* suggests that chromodomain protein binding to RNA antagonizes recognition of methylated histone [77, 78]. It is possible that the Mst1 effect on heterochromatin silencing or CPT response is mediated by an RNA binding function of the chromodomain.

Materials and methods

Strains and media

Fission yeast cells were grown in YES (yeast extract with supplements) or PMG (pombe minimal glutamate) with appropriate supplements [79]. Yeast strains used in this research are listed in S1 Table in the supplemental material.

Construction of *mst1-W66R*

mst1-W66R was made by site-directed mutagenesis using Phusion Site-Directed Mutagenesis Kit with primers 5'Phos/CGTTTAGATGAAAGGATTACAATAGAT (Forward) and 5'Phos/TTTATTGTAGCATTATAGTG (Reverse). The *mst1-W66R* sequence was then cloned into pEBG78 (pTZ*ura4*$^+$ 5'/3'UTR *mst1* (construct to disrupt *mst1*$^+$ with *ura4*$^+$). *mst1-W66R* construct was then PCR amplified and transformed into genome.

Serial dilution plating

Yeast cell cultures were grown at 32˚C in YES for one day. Cultures were diluted in YES to equal concentrations. Five-fold serial dilutions of the cultures were then spotted onto YES plates containing different concentrations of drugs. Plates were incubated at 32˚C or 36˚C for four days before scanning.

Silencing assay

Silencing assays were performed as described previously [80] with the following modifications. Cells were grown to mid-log phase to 5X10^6 cells/ml and spotted on selective medium with 1:5 serial dilutions. For *ura4*$^+$ expression, cells were spotted on YES or non-selective with 1 g/L of 5' FOA. Cells were grown at 32˚C or 36˚C for 4 days.

RT-PCR

RT-PCR was performed as described previously [50]. Cells were grown to mid-log phase. Total RNA was extracted using Qiagen RNeasy isolation kit according to manufacturer's instructions and treated with TURBO DNA-free kit following routine DNase treatment instructions. Total RNA was resuspended in TE and checked for integrity by agarose electrophoresis. The cDNA strand was synthesized with 1μg RNA using Invitrogen SuperScript First-strand cDNA synthesis kit following the manufacturer's instructions. The amount of *ura4*$^+$ RNA expression was determined by PCR and analyzed by Amersham Typhoon laser and Fiji ImageJ. Three biological replicates were assessed for consistency. Results were plotted as fold expression relative to the mini-gene *ura4*-DS/E, located at the endogenous *ura4*$^+$ locus.

Live-cell imaging and quantitative measurements

Live cells imaging was performed as described in [81]. Yeast cell cultures were grown at 32˚C in YES overnight. Cells were transferred into PMG + HULAA (Histidine, Uracil, Leucine, Adenine, Arginine) liquid cultures at 36˚C for 16 hours before treating with 5μg/mL camptothecin for four hours. Cells were collected at OD_{595} 0.3–0.6, concentrated by centrifuging 1ml at 1500g for 1min and resuspended in 40μl. Concentrated cells were placed on a thin-film pad of 2% agarose in PMG+HULAA on a glass slide. A coverslip was added. Live cells were imaged on DeltaVision Core microscope with softWoRx v4.1 (GE, Issaquah, WA), using a 60X lens, and then deconvolved and projected in softWoRx software. Images were acquired in 13 0.2μm z-sections, then deconvolved and Maximum Intensity Projected (softWoRx, default settings). Two separate fields were imaged in each experiment, and 2 to 4 biological replicates were assessed for consistency. Images for publication were contrast adjusted using an equivalent histogram stretch on all samples. Color balance was adjusted, and scale bars were added in Fiji [82]. Significance was calculated using the Mann-Whitney U test.

LacO LacI-mCherry DSB array colocalization with CFP-tagged Rad52

The assay was performed as described in [42]. In this system, the HO endonuclease is driven by the nmt1 promoter, which takes approximately 20 hours to induce following removal of thiamine from the media [83]. The assay can quantitively monitor resection and DSB repair factors recruitment to the break. A difference in fluorescent signal between WT controls and mutants demonstrates a resection and recruitment failure. Cells were cultured at 36˚C in PMG + HULAA + Thiamine liquid media to OD595 of 0.4–0.6. Cells were then washed twice with PMG + HULAA medium and incubated at 36˚C for 19 hours to induce the HO-driven DSB break. Following induction, cells were collected at OD595 of 0.3–0.6, and were processed and imaged as described above.

mRNA sequencing and gene expression analysis

Yeast cell cultures were grown at 36˚C for one day before treating with 15μM camptothecin for four hours. RNA was isolated from yeast cell culture using the Qiagen RNeasy kit according to manufactures instructions. 200 ng of RNA was used for gene expression analysis with NovaSeq PE150. Sequence reads quality was checked using FastQC 0.11.7. Sequence reads were then aligned using STARalign 2.7.0e and assembled using Cufflinks 2.2.1.

The counts were normalized using housekeeping genes (act1, adh1, atb2 and gad8) as control with methods in "RUVseq" package in R [84]. Downstream filtering, normalization, dispersion and model fitting, as well as differential expression were performed with "edgeR" package in R [85]. Multidimensional analysis and principal component analysis were performed using normalized counts-per-million generated using "cpm" function in "edgeR" to visualize sample variation, as well as to identify potential sample outliers and gene outliers respectively. Over-expression and gene set enrichment analysis were performed using R package "clusterProfiler" [86]. p-value cut-off was set to 0.05 for GO over-representation test and Kyoto Encyclopedia of Genes and Genomes (KEGG) over-representation test, 0.3 for GO gene set enrichment analysis (GSEA). Gene list for GSEA were prepared based on the order of log2 (Fold change).

Supporting information

S1 Fig. The conserved chromodomain sequences. Chromodomain sequences of the indicated coordinates were aligned using Clustal Omega-Multiple Sequence Alignment. All sequences

are for strain 972h- from PomBase.
(TIF)

S2 Fig. *mst1-W66R* mutant characterization in transcriptome. (A)-(B) Volcano plot of differentially expressed genes (p-value cutoff = 0.05, log2(Fold change) cutoff = 1.5) in (A) untreated *mst1-W66R* compared to untreated wild type. (B) CPT treated *mst1-W66R* compared to untreated *mst1-W66R*. (C)-(D) KEGG analysis of (C) upregulated and (D) downregulated pathways in CPT treated *mst1-W66R* compared to untreated *mst1-W66R*.
(TIF)

S3 Fig. *mst1-W66R* mutants sensitivity to CPT are temperature specific and *mst1-W66R* is a dominant negative allele. (A) *clr4Δ*, *swi6Δ*, *dcr1Δ* and the double mutants with *mst1-W66R* showed sensitivity to CPT at 32˚C. (B) *mst1-W66R* cells complemented with plasmid expressing wild type Mst1 under native promoter. Cells were grown in YES media overnight at 32˚C then 5X serial dilutions were spotted onto YES plates or YES plates containing CPT. Plates were incubated at 32˚C or 36˚C and photographed after 4 days.
(TIF)

S4 Fig. *mst1-W66R* affects the repair of CPT-induced damages genome-wide. Top: Percentage of cells with single focus or multi-foci of (A) RPA (Rad11) (B) Rad52 and (C) Rad54 foci in WT, *mst1-W66R*, *rad2Δ*, *rad2Δ mst1-W66R*, *rad16Δ*, *rad16Δ mst1-W66R* and *rad2Δ rad16Δ*. **Bottom:** Examples of cells with multi-foci after CPT treatment. Rad11-CFP is colored magenta for visibility.
(TIF)

S1 Raw images. Raw images of Fig 4.
(PDF)

S1 Table. Strains used in this study.
(XLSX)

S2 Table. Differential-expressed genes from mRNA-sequencing.
(XLSX)

S3 Table. Average ± standard error of cells with Rad11, Rad52 or Rad54 shown in Fig 5.
(XLSX)

Acknowledgments

We thank Takuro Nakagawa, Eishi Noguchi, Li-Lin Du, Robin Allshire, Yota Murakami and Karl Ekwall for providing strains. We thank Ji-Ping Yuan for assistance and technical support. We are grateful to current members of the Forsburg lab for many helpful comments and discussions throughout the course of the study, and an anonymous reviewer for helpful suggestion.

Author Contributions

Conceptualization: Tingting Li, Ruben C. Petreaca, Susan L. Forsburg.

Data curation: Tingting Li, Ruben C. Petreaca.

Formal analysis: Tingting Li, Susan L. Forsburg.

Funding acquisition: Susan L. Forsburg.

Investigation: Tingting Li.

Methodology: Tingting Li.

Project administration: Susan L. Forsburg.

Software: Tingting Li.

Supervision: Susan L. Forsburg.

Validation: Tingting Li.

Visualization: Tingting Li.

Writing – original draft: Tingting Li, Susan L. Forsburg.

Writing – review & editing: Tingting Li, Ruben C. Petreaca, Susan L. Forsburg.

References

1. Utley R.T.; Cote J. The MYST family of histone acetyltransferases. *Curr Top Microbiol Immunol* 2003, 274, 203–236, https://doi.org/10.1007/978-3-642-55747-7_8 PMID: 12596909
2. Thomas T.; Voss A.K. The diverse biological roles of MYST histone acetyltransferase family proteins. *Cell Cycle* 2007, 6, 696–704, https://doi.org/10.4161/cc.6.6.4013 PMID: 17374998
3. Avvakumov N.; Cote J. The MYST family of histone acetyltransferases and their intimate links to cancer. *Oncogene* 2007, 26, 5395–5407, https://doi.org/10.1038/sj.onc.1210608 PMID: 17694081
4. Pillus L. MYSTs mark chromatin for chromosomal functions. *Curr Opin Cell Biol* 2008, 20, 326–333, https://doi.org/10.1016/j.ceb.2008.04.009 PMID: 18511253
5. Sapountzi V.; Logan I.R.; Robson C.N. Cellular functions of TIP60. *Int J Biochem Cell Biol* 2006, 38, 1496–1509, https://doi.org/10.1016/j.biocel.2006.03.003 PMID: 16698308
6. Voss A.K.; Thomas T. MYST family histone acetyltransferases take center stage in stem cells and development. *Bioessays* 2009, 31, 1050–1061, https://doi.org/10.1002/bies.200900051 PMID: 19722182
7. Judes G.; Rifai K.; Ngollo M.; Daures M.; Bignon Y.J.; Penault-Llorca F.; Bernard-Gallon D. A bivalent role of TIP60 histone acetyl transferase in human cancer. *Epigenomics* 2015, 7, 1351–1363, https://doi.org/10.2217/epi.15.76 PMID: 26638912
8. Doyon Y.; Cote J. The highly conserved and multifunctional NuA4 HAT complex. *Curr Opin Genet Dev* 2004, 14, 147–154, https://doi.org/10.1016/j.gde.2004.02.009 PMID: 15196461
9. Scacchetti A.; Becker P.B. Variation on a theme: Evolutionary strategies for H2A.Z exchange by SWR1-type remodelers. *Curr Opin Cell Biol* 2021, 70, 1–9, https://doi.org/10.1016/j.ceb.2020.10.014 PMID: 33217681
10. Sun Y.; Xu Y.; Roy K.; Price B.D. DNA damage-induced acetylation of lysine 3016 of ATM activates ATM kinase activity. *Mol Cell Biol* 2007, 27, 8502–8509, https://doi.org/10.1128/MCB.01382-07 PMID: 17923702
11. Cheng X.; Jobin-Robitaille O.; Billon P.; Buisson R.; Niu H.; Lacoste N.; et al. Phospho-dependent recruitment of the yeast NuA4 acetyltransferase complex by MRX at DNA breaks regulates RPA dynamics during resection. *Proc Natl Acad Sci U S A* 2018, 115, 10028–10033, https://doi.org/10.1073/pnas.1806513115 PMID: 30224481
12. Grezy A.; Chevillard-Briet M.; Trouche D.; Escaffit F. Control of genetic stability by a new heterochromatin compaction pathway involving the Tip60 histone acetyltransferase. *Mol Biol Cell* 2016, 27, 599–607, https://doi.org/10.1091/mbc.E15-05-0316 PMID: 26700317
13. Xhemalce B.; Kouzarides T. A chromodomain switch mediated by histone H3 Lys 4 acetylation regulates heterochromatin assembly. *Genes Dev* 2010, 24, 647–652, https://doi.org/10.1101/gad.1881710 PMID: 20299449
14. Gomez E.B.; Nugent R.L.; Laria S.; Forsburg S.L. Schizosaccharomyces pombe histone acetyltransferase Mst1 (KAT5) is an essential protein required for damage response and chromosome segregation. *Genetics* 2008, 179, 757–771, https://doi.org/10.1534/genetics.107.085779 PMID: 18505873
15. Taverna S.D.; Li H.; Ruthenburg A.J.; Allis C.D.; Patel D.J. How chromatin-binding modules interpret histone modifications: lessons from professional pocket pickers. *Nat Struct Mol Biol* 2007, 14, 1025–1040, https://doi.org/10.1038/nsmb1338 PMID: 17984965

16. Ayrapetov M.K.; Gursoy-Yuzugullu O.; Xu C.; Xu Y.; Price B.D. DNA double-strand breaks promote methylation of histone H3 on lysine 9 and transient formation of repressive chromatin. *Proc Natl Acad Sci U S A* 2014, 111, 9169–9174, https://doi.org/10.1073/pnas.1403565111 PMID: 24927542

17. Li T.; Petreaca R.C.; Forsburg S.L. Schizosaccharomyces pombe KAT5 contributes to resection and repair of a DNA double-strand break. *Genetics* 2021, 218, https://doi.org/10.1093/genetics/iyab042 PMID: 33723569

18. K L.H.; T M.H.; R A.B.; R C.P. KAT5 histone acetyltransferase mutations in cancer cells. *MicroPubl Biol* 2022, 2022, https://doi.org/10.17912/micropub.biology.000676 PMID: 36530474

19. Morillo-Huesca M.; Clemente-Ruiz M.; Andujar E.; Prado F. The SWR1 histone replacement complex causes genetic instability and genome-wide transcription misregulation in the absence of H2A.Z. *PLoS One* 2010, 5, e12143, https://doi.org/10.1371/journal.pone.0012143 PMID: 20711347

20. Papamichos-Chronakis M.; Watanabe S.; Rando O.J.; Peterson C.L. Global regulation of H2A.Z localization by the INO80 chromatin-remodeling enzyme is essential for genome integrity. *Cell* 2011, 144, 200–213, https://doi.org/10.1016/j.cell.2010.12.021 PMID: 21241891

21. Xu Y.; Ayrapetov M.K.; Xu C.; Gursoy-Yuzugullu O.; Hu Y.; Price B.D. Histone H2A.Z controls a critical chromatin remodeling step required for DNA double-strand break repair. *Mol Cell* 2012, 48, 723–733, https://doi.org/10.1016/j.molcel.2012.09.026 PMID: 23122415

22. Gursoy-Yuzugullu O.; Ayrapetov M.K.; Price B.D. Histone chaperone Anp32e removes H2A.Z from DNA double-strand breaks and promotes nucleosome reorganization and DNA repair. *Proc Natl Acad Sci U S A* 2015, 112, 7507–7512, https://doi.org/10.1073/pnas.1504868112 PMID: 26034280

23. Bird A.W.; Yu D.Y.; Pray-Grant M.G.; Qiu Q.; Harmon K.E.; Megee P.C.; et al. Acetylation of histone H4 by Esa1 is required for DNA double-strand break repair. *Nature* 2002, 419, 411–415, https://doi.org/10.1038/nature01035 PMID: 12353039

24. Downs J.A.; Allard S.; Jobin-Robitaille O.; Javaheri A.; Auger A.; Bouchard N.; et al. Binding of chromatin-modifying activities to phosphorylated histone H2A at DNA damage sites. *Mol Cell* 2004, 16, 979–990, https://doi.org/10.1016/j.molcel.2004.12.003 PMID: 15610740

25. Doyon Y.; Selleck W.; Lane W.S.; Tan S.; Cote J. Structural and functional conservation of the NuA4 histone acetyltransferase complex from yeast to humans. *Mol Cell Biol* 2004, 24, 1884–1896, https://doi.org/10.1128/MCB.24.5.1884-1896.2004 PMID: 14966270

26. Murr R.; Loizou J.I.; Yang Y.G.; Cuenin C.; Li H.; Wang Z.Q.; et al. Histone acetylation by Trrap-Tip60 modulates loading of repair proteins and repair of DNA double-strand breaks. *Nat Cell Biol* 2006, 8, 91–99, https://doi.org/10.1038/ncb1343 PMID: 16341205

27. Clarke T.L.; Sanchez-Bailon M.P.; Chiang K.; Reynolds J.J.; Herrero-Ruiz J.; Bandeiras T.M.; et al. PRMT5-Dependent Methylation of the TIP60 Coactivator RUVBL1 Is a Key Regulator of Homologous Recombination. *Mol Cell* 2017, 65, 900–916 e907, https://doi.org/10.1016/j.molcel.2017.01.019 PMID: 28238654

28. Ikura T.; Tashiro S.; Kakino A.; Shima H.; Jacob N.; Amunugama R.; et al. DNA damage-dependent acetylation and ubiquitination of H2AX enhances chromatin dynamics. *Mol Cell Biol* 2007, 27, 7028–7040, https://doi.org/10.1128/MCB.00579-07 PMID: 17709392

29. Sharma G.G.; So S.; Gupta A.; Kumar R.; Cayrou C.; Avvakumov N.; et al. MOF and histone H4 acetylation at lysine 16 are critical for DNA damage response and double-strand break repair. *Mol Cell Biol* 2010, 30, 3582–3595, https://doi.org/10.1128/MCB.01476-09 PMID: 20479123

30. Jha S.; Shibata E.; Dutta A. Human Rvb1/Tip49 is required for the histone acetyltransferase activity of Tip60/NuA4 and for the downregulation of phosphorylation on H2AX after DNA damage. *Mol Cell Biol* 2008, 28, 2690–2700, https://doi.org/10.1128/MCB.01983-07 PMID: 18285460

31. Soria G.; Polo S.E.; Almouzni G. Prime, repair, restore: the active role of chromatin in the DNA damage response. *Mol Cell* 2012, 46, 722–734, https://doi.org/10.1016/j.molcel.2012.06.002 PMID: 22749398

32. Renaud E.; Barascu A.; Rosselli F. Impaired TIP60-mediated H4K16 acetylation accounts for the aberrant chromatin accumulation of 53BP1 and RAP80 in Fanconi anemia pathway-deficient cells. *Nucleic Acids Res* 2016, 44, 648–656, https://doi.org/10.1093/nar/gkv1019 PMID: 26446986

33. Jacquet K.; Fradet-Turcotte A.; Avvakumov N.; Lambert J.P.; Roques C.; Pandita R.K.; et al. The TIP60 Complex Regulates Bivalent Chromatin Recognition by 53BP1 through Direct H4K20me Binding and H2AK15 Acetylation. *Mol Cell* 2016, 62, 409–421, https://doi.org/10.1016/j.molcel.2016.03.031 PMID: 27153538

34. Noguchi C.; Singh T.; Ziegler M.A.; Peake J.D.; Khair L.; Aza A.; et al. The NuA4 acetyltransferase and histone H4 acetylation promote replication recovery after topoisomerase I-poisoning. *Epigenetics Chromatin* 2019, 12, 24, https://doi.org/10.1186/s13072-019-0271-z PMID: 30992049

35. Decker P.V.; Yu D.Y.; Iizuka M.; Qiu Q.; Smith M.M. Catalytic-site mutations in the MYST family histone Acetyltransferase Esa1. *Genetics* 2008, 178, 1209–1220, https://doi.org/10.1534/genetics.107.080135 PMID: 18245364

36. Sun Y.; Jiang X.; Chen S.; Fernandes N.; Price B.D. A role for the Tip60 histone acetyltransferase in the acetylation and activation of ATM. *Proc Natl Acad Sci U S A* 2005, 102, 13182–13187, https://doi.org/10.1073/pnas.0504211102 PMID: 16141325

37. Sun Y.; Jiang X.; Xu Y.; Ayrapetov M.K.; Moreau L.A.; Whetstine J.R.; et al. Histone H3 methylation links DNA damage detection to activation of the tumour suppressor Tip60. *Nat Cell Biol* 2009, 11, 1376–1382, https://doi.org/10.1038/ncb1982 PMID: 19783983

38. Ghobashi A.H.; Kamel M.A. Tip60: updates. *J Appl Genet* 2018, 59, 161–168, https://doi.org/10.1007/s13353-018-0432-y PMID: 29549519

39. Thomas A.; Pommier Y. Targeting Topoisomerase I in the Era of Precision Medicine. *Clin Cancer Res* 2019, 25, 6581–6589, https://doi.org/10.1158/1078-0432.CCR-19-1089 PMID: 31227499

40. Lin C.P.; Ban Y.; Lyu Y.L.; Liu L.F. Proteasome-dependent processing of topoisomerase I-DNA adducts into DNA double strand breaks at arrested replication forks. *J Biol Chem* 2009, 284, 28084–28092, https://doi.org/10.1074/jbc.M109.030601 PMID: 19666469

41. Cristini A.; Ricci G.; Britton S.; Salimbeni S.; Huang S.N.; Marinello J.; et al. Dual Processing of R-Loops and Topoisomerase I Induces Transcription-Dependent DNA Double-Strand Breaks. *Cell Rep* 2019, 28, 3167–3181 e3166, https://doi.org/10.1016/j.celrep.2019.08.041 PMID: 31533039

42. Yu Y.; Ren J.Y.; Zhang J.M.; Suo F.; Fang X.F.; Wu F.; et al. A proteome-wide visual screen identifies fission yeast proteins localizing to DNA double-strand breaks. *DNA Repair (Amst)* 2013, 12, 433–443, https://doi.org/10.1016/j.dnarep.2013.04.001 PMID: 23628481

43. Li P.; Li J.; Li M.; Dou K.; Zhang M.J.; Suo F.; et al. Multiple end joining mechanisms repair a chromosomal DNA break in fission yeast. *DNA Repair (Amst)* 2012, 11, 120–130, https://doi.org/10.1016/j.dnarep.2011.10.011 PMID: 22093869

44. Nugent R.L.; Johnsson A.; Fleharty B.; Gogol M.; Xue-Franzen Y.; Seidel C.; et al. Expression profiling of S. pombe acetyltransferase mutants identifies redundant pathways of gene regulation. *BMC Genomics* 2010, 11, 59, https://doi.org/10.1186/1471-2164-11-59 PMID: 20096118

45. Allshire R.C.; Ekwall K. Epigenetic Regulation of Chromatin States in Schizosaccharomyces pombe. *Cold Spring Harb Perspect Biol* 2015, 7, a018770, https://doi.org/10.1101/cshperspect.a018770 PMID: 26134317

46. Nakagawa T.; Okita A.K. Transcriptional silencing of centromere repeats by heterochromatin safeguards chromosome integrity. *Curr Genet* 2019, 65, 1089–1098, https://doi.org/10.1007/s00294-019-00975-x PMID: 30997531

47. Allshire R.C.; Javerzat J.P.; Redhead N.J.; Cranston G. Position effect variegation at fission yeast centromeres. *Cell* 1994, 76, 157–169, https://doi.org/10.1016/0092-8674(94)90180-5 PMID: 8287474

48. Kloc A.; Zaratiegui M.; Nora E.; Martienssen R. RNA interference guides histone modification during the S phase of chromosomal replication. *Curr Biol* 2008, 18, 490–495, https://doi.org/10.1016/j.cub.2008.03.016 PMID: 18394897

49. Ekwall K.; Javerzat J.P.; Lorentz A.; Schmidt H.; Cranston G.; Allshire R. The chromodomain protein Swi6: a key component at fission yeast centromeres. *Science* 1995, 269, 1429–1431, https://doi.org/10.1126/science.7660126 PMID: 7660126

50. Li P.C.; Chretien L.; Cote J.; Kelly T.J.; Forsburg S.L. S. pombe replication protein Cdc18 (Cdc6) interacts with Swi6 (HP1) heterochromatin protein: region specific effects and replication timing in the centromere. *Cell Cycle* 2011, 10, 323–336, https://doi.org/10.4161/cc.10.2.14552 PMID: 21239883

51. Bannister A.J.; Zegerman P.; Partridge J.F.; Miska E.A.; Thomas J.O.; Allshire R.C.; et al. Selective recognition of methylated lysine 9 on histone H3 by the HP1 chromo domain. *Nature* 2001, 410, 120–124, https://doi.org/10.1038/35065138 PMID: 11242054

52. Ivanova A.V.; Bonaduce M.J.; Ivanov S.V.; Klar A.J. The chromo and SET domains of the Clr4 protein are essential for silencing in fission yeast. *Nat Genet* 1998, 19, 192–195, https://doi.org/10.1038/566 PMID: 9620780

53. Volpe T.; Schramke V.; Hamilton G.L.; White S.A.; Teng G.; Martienssen R.A.; et al. RNA interference is required for normal centromere function in fission yeast. *Chromosome Res* 2003, 11, 137–146, https://doi.org/10.1023/a:1022815931524 PMID: 12733640

54. Woolcock K.J.; Stunnenberg R.; Gaidatzis D.; Hotz H.R.; Emmerth S.; Barraud P.; et al. RNAi keeps Atf1-bound stress response genes in check at nuclear pores. *Genes Dev* 2012, 26, 683–692, https://doi.org/10.1101/gad.186866.112 PMID: 22431512

55. Jalan M.; Olsen K.S.; Powell S.N. Emerging Roles of RAD52 in Genome Maintenance. *Cancers (Basel)* 2019, 11, https://doi.org/10.3390/cancers11071038 PMID: 31340507

56. Sugiyama T.; Kowalczykowski S.C. Rad52 protein associates with replication protein A (RPA)-single-stranded DNA to accelerate Rad51-mediated displacement of RPA and presynaptic complex formation. *J Biol Chem* 2002, 277, 31663–31672, https://doi.org/10.1074/jbc.M203494200 PMID: 12077133

57. Bugreev D.V.; Rossi M.J.; Mazin A.V. Cooperation of RAD51 and RAD54 in regression of a model replication fork. *Nucleic Acids Res* 2011, 39, 2153–2164, https://doi.org/10.1093/nar/gkq1139 PMID: 21097884

58. Tsutsui Y.; Khasanov F.K.; Shinagawa H.; Iwasaki H.; Bashkirov V.I. Multiple interactions among the components of the recombinational DNA repair system in Schizosaccharomyces pombe. *Genetics* 2001, 159, 91–105, https://doi.org/10.1093/genetics/159.1.91 PMID: 11560889

59. Ben Hassine S.; Arcangioli B. Tdp1 protects against oxidative DNA damage in non-dividing fission yeast. *EMBO J* 2009, 28, 632–640, https://doi.org/10.1038/emboj.2009.9 PMID: 19197239

60. Paull T.T.; Gellert M. The 3' to 5' exonuclease activity of Mre 11 facilitates repair of DNA double-strand breaks. *Mol Cell* 1998, 1, 969–979, https://doi.org/10.1016/s1097-2765(00)80097-0 PMID: 9651580

61. Regairaz M.; Zhang Y.W.; Fu H.; Agama K.K.; Tata N.; Agrawal S.; et al. Mus81-mediated DNA cleavage resolves replication forks stalled by topoisomerase I-DNA complexes. *J Cell Biol* 2011, 195, 739–749, https://doi.org/10.1083/jcb.201104003 PMID: 22123861

62. Carr A.M.; Schmidt H.; Kirchhoff S.; Muriel W.J.; Sheldrick K.S.; Griffiths D.J.; et al. The rad16 gene of Schizosaccharomyces pombe: a homolog of the RAD1 gene of Saccharomyces cerevisiae. *Mol Cell Biol* 1994, 14, 2029–2040, https://doi.org/10.1128/mcb.14.3.2029-2040.1994 PMID: 8114734

63. Lafon A.; Chang C.S.; Scott E.M.; Jacobson S.J.; Pillus L. MYST opportunities for growth control: yeast genes illuminate human cancer gene functions. *Oncogene* 2007, 26, 5373–5384, https://doi.org/10.1038/sj.onc.1210606 PMID: 17694079

64. Alleva J.L.; Doetsch P.W. The nature of the 5'-terminus is a major determinant for DNA processing by Schizosaccharomyces pombe Rad2p, a FEN-1 family nuclease. *Nucleic Acids Res* 2000, 28, 2893–2901, https://doi.org/10.1093/nar/28.15.2893 PMID: 10908351

65. Smith E.R.; Eisen A.; Gu W.; Sattah M.; Pannuti A.; Zhou J.; et al. ESA1 is a histone acetyltransferase that is essential for growth in yeast. *Proc Natl Acad Sci U S A* 1998, 95, 3561–3565, https://doi.org/10.1073/pnas.95.7.3561 PMID: 9520405

66. Wan S.; Capasso H.; Walworth N.C. The topoisomerase I poison camptothecin generates a Chk1-dependent DNA damage checkpoint signal in fission yeast. *Yeast* 1999, 15, 821–828, https://doi.org/10.1002/(SICI)1097-0061(199907)15:10A<821::AID-YEA422>3.0.CO;2-# PMID: 10407262

67. Li P.C.; Petreaca R.C.; Jensen A.; Yuan J.P.; Green M.D.; Forsburg S.L. Replication fork stability is essential for the maintenance of centromere integrity in the absence of heterochromatin. *Cell Rep* 2013, 3, 638–645, https://doi.org/10.1016/j.celrep.2013.02.007 PMID: 23478021

68. Ekwall K.; Nimmo E.R.; Javerzat J.P.; Borgstrom B.; Egel R.; Cranston G.; et al. Mutations in the fission yeast silencing factors clr4+ and rik1+ disrupt the localisation of the chromo domain protein Swi6p and impair centromere function. *J Cell Sci* 1996, 109 (Pt 11), 2637–2648, https://doi.org/10.1242/jcs.109.11.2637 PMID: 8937982

69. Baranello L.; Bertozzi D.; Fogli M.V.; Pommier Y.; Capranico G. DNA topoisomerase I inhibition by camptothecin induces escape of RNA polymerase II from promoter-proximal pause site, antisense transcription and histone acetylation at the human HIF-1alpha gene locus. *Nucleic Acids Res* 2010, 38, 159–171, https://doi.org/10.1093/nar/gkp817 PMID: 19854946

70. Zaratiegui M.; Castel S.E.; Irvine D.V.; Kloc A.; Ren J.; Li F.; et al. RNAi promotes heterochromatic silencing through replication-coupled release of RNA Pol II. *Nature* 2011, 479, 135–138, https://doi.org/10.1038/nature10501 PMID: 22002604

71. Sabatinos S.A.; Forsburg S.L. Managing Single-Stranded DNA during Replication Stress in Fission Yeast. *Biomolecules* 2015, 5, 2123–2139, https://doi.org/10.3390/biom5032123 PMID: 26393661

72. Brustel J.; Kozik Z.; Gromak N.; Savic V.; Sweet S.M.M. Large XPF-dependent deletions following misrepair of a DNA double strand break are prevented by the RNA:DNA helicase Senataxin. *Sci Rep* 2018, 8, 3850, https://doi.org/10.1038/s41598-018-21806-y PMID: 29497062

73. Kim C.H.; Kim J.W.; Jang S.M.; An J.H.; Seo S.B.; Choi K.H. The chromodomain-containing histone acetyltransferase TIP60 acts as a code reader, recognizing the epigenetic codes for initiating transcription. *Biosci Biotechnol Biochem* 2015, 79, 532–538, https://doi.org/10.1080/09168451.2014.993914 PMID: 25560918

74. Pfister S.X.; Ahrabi S.; Zalmas L.P.; Sarkar S.; Aymard F.; Bachrati C.Z.; et al. SETD2-dependent histone H3K36 trimethylation is required for homologous recombination repair and genome stability. *Cell Rep* 2014, 7, 2006–2018, https://doi.org/10.1016/j.celrep.2014.05.026 PMID: 24931610

75. Shimojo H.; Sano N.; Moriwaki Y.; Okuda M.; Horikoshi M.; Nishimura Y. Novel structural and functional mode of a knot essential for RNA binding activity of the Esa1 presumed chromodomain. *J Mol Biol* 2008, 378, 987–1001, https://doi.org/10.1016/j.jmb.2008.03.021 PMID: 18407291

76. Jacobs S.A.; Taverna S.D.; Zhang Y.; Briggs S.D.; Li J.; Eissenberg J.C.; et al. Specificity of the HP1 chromo domain for the methylated N-terminus of histone H3. *EMBO J* 2001, 20, 5232–5241, https://doi.org/10.1093/emboj/20.18.5232 PMID: 11566886

77. Ren J.; Martienssen R.A. Silent decision: HP1 protein escorts heterochromatic RNAs to their destiny. *EMBO J* 2012, 31, 3237–3238, https://doi.org/10.1038/emboj.2012.172 PMID: 22705945

78. Ishida M.; Shimojo H.; Hayashi A.; Kawaguchi R.; Ohtani Y.; Uegaki K.; et al. Intrinsic nucleic acid-binding activity of Chp1 chromodomain is required for heterochromatic gene silencing. *Mol Cell* 2012, 47, 228–241, https://doi.org/10.1016/j.molcel.2012.05.017 PMID: 22727667

79. Sabatinos S.A.; Forsburg S.L. Molecular genetics of Schizosaccharomyces pombe. *Methods Enzymol* 2010, 470, 759–795, https://doi.org/10.1016/S0076-6879(10)70032-X PMID: 20946835

80. Freeman-Cook L.L.; Gomez E.B.; Spedale E.J.; Marlett J.; Forsburg S.L.; Pillus L.; et al. Conserved locus-specific silencing functions of Schizosaccharomyces pombe sir2+. *Genetics* 2005, 169, 1243–1260, https://doi.org/10.1534/genetics.104.032714 PMID: 15545655

81. Green M.D.; Sabatinos S.A.; Forsburg S.L. Microscopy techniques to examine DNA replication in fission yeast. *Methods Mol Biol* 2009, 521, 463–482, https://doi.org/10.1007/978-1-60327-815-7_26 PMID: 19563123

82. Schindelin J.; Arganda-Carreras I.; Frise E.; Kaynig V.; Longair M.; Pietzsch T.; et al. Fiji: an open-source platform for biological-image analysis. *Nat Methods* 2012, 9, 676–682, https://doi.org/10.1038/nmeth.2019 PMID: 22743772

83. Forsburg S.L. Comparison of Schizosaccharomyces pombe expression systems. *Nucleic Acids Res* 1993, 21, 2955–2956, https://doi.org/10.1093/nar/21.12.2955 PMID: 8332516

84. Risso D.; Ngai J.; Speed T.P.; Dudoit S. Normalization of RNA-seq data using factor analysis of control genes or samples. *Nat Biotechnol* 2014, 32, 896–902, https://doi.org/10.1038/nbt.2931 PMID: 25150836

85. McCarthy D.J.; Chen Y.; Smyth G.K. Differential expression analysis of multifactor RNA-Seq experiments with respect to biological variation. *Nucleic Acids Res* 2012, 40, 4288–4297, https://doi.org/10.1093/nar/gks042 PMID: 22287627

86. Yu G.; Wang L.G.; Han Y.; He Q.Y. clusterProfiler: an R package for comparing biological themes among gene clusters. *OMICS* 2012, 16, 284–287, https://doi.org/10.1089/omi.2011.0118 PMID: 22455463